Int. J. Solids Structures, 1974, Vol. 10, pp. 1243–1269. Pergamon Press. Printed in Gt. Britain

ON THE STRESS PROBLEM OF LARGE ELLIPTICAL CUTOUTS AND CRACKS IN CIRCULAR CYLINDRICAL SHELLS

M. V. V. MURTHY†
Structures Division, National Aeronautical Laboratory, Bangalore, India.

K. P. RAO‡ and A. K. RAO§
Department of Aeronautical Engineering, Indian Institute of Science, Bangalore, India.

(*Received* 7 *September* 1973; *revised* 18 *March* 1974)

Abstract—Numerical solutions are presented for stresses around an elliptical hole in a long, thin, circular cylindrical shell subjected to axial tension for both the symmetric orientations of the hole with respect to the shell. The method of analysis involves obtaining a series solution to the governing shell equations in terms of Mathieu functions by the method of separation of variables and satisfying the boundary conditions numerically term by term in a Fourier series formulation. Results are presented in the form of charts from which stress concentration factors can be directly read over a wide range of the two parameters, namely, axis ratio of the ellipse and a curvature parameter defining the hole size with respect to dimensions of the shell.

An interesting feature of the investigation is the analysis of limiting cases of circumferential and axial cracks for axial tension and internal pressure loadings respectively. The method developed involves determining the solution completely in elliptic coordinates and then determining the singular stresses by carrying out a transformation to polar coordinates with crack tip as the origin through a Taylor series expansion. Membrane and bending stress intensity factors are computed and plotted over a sufficiently wide range of the curvature parameter extending from small to large sized cracks. As an outcome of the analysis, a "hybrid" technique has been developed by which singularity conditions at the crack tip can be handled effectively in dealing with boundary conditions in crack problems.

NOMENCLATURE

R, t	Radius and thickness of shell, respectively, Fig. 1
$2a, 2b$	lengths of major and minor axes, respectively, Figs. 1 and 2
k	axis ratio of the ellipse, b/a
ε	out-of-roundness parameter, $(a-b)/(a+b)$
$2h$	interfocal distance nondimensionalized with respect to a, Fig. 2
ν	Poisson's ratio
E	Young's modulus
β	a dimensionless curvature parameter, $\beta^2 = a^2[12(1-\nu^2)]^{1/2}/8Rt$
X, Y	rectangular coordinates with X axis oriented along major axis of the ellipse and nondimensionalized with respect to a, Figs. 1 and 2
x, y	rectangular coordinates with x axis oriented along the shell axis and nondimensionalized with respect to a, Fig. 1
r, θ	polar coordinates with crack tip as the origin, r being nondimensionalized with respect to a, Fig. 1

† Scientist.
‡ Assistant professor.
§ Professor.

ξ, η elliptic coordinates, Fig. 2
K nondimensional scale factor for elliptic coordinates, $[h^2(\cosh 2\xi - \cos 2\eta)/2]^{1/2}$
σ uniform stress in the shell at large distances from the hole
W displacement normal to middle surface of shell, positive radially outward and nondimensionalized with respect to $\sigma a^2[12(1-\nu^2)]^{1/2}/Et$, Fig. 2
Φ stress function nondimensionalized with respect to $\sigma t a^2$
F nondimensional complex function,

$$(W - i\Phi),\ i = \sqrt{-1}$$

$N_\xi, N_\eta, N_{\xi\eta}$
$N_r, N_\theta, N_{r\theta}$ membrane forces in elliptic and polar coordinates respectively, nondimensionalized with respect to σt, Fig. 2
$M_\xi, M_\eta, M_{\xi\eta}$
$M_r, M_\theta, M_{r\theta}$ bending moments in elliptic and polar coordinates respectively, nondimensionalized with respect to $\sigma t^2/[12(1-\nu^2)]^{1/2}$, Fig. 2
Q_ξ, Q_η
Q_r, Q_θ transverse shear forces in elliptic and polar coordinates respectively, nondimensionalized with respect to $\sigma t^2/a[12(1-\nu^2)]^{1/2}$, Fig. 2
$\bar{Q}_\xi, \bar{Q}_\eta$
$\bar{Q}_r, \bar{Q}_\theta$ Kirchhoff shears in elliptic and polar coordinates respectively, nondimensionalized with respect to $\sigma t^2/a[12(1-\nu^2)]^{1/2}$
$\sigma_\xi, \sigma_\eta, \tau_{\xi\eta}$
$\sigma_r, \sigma_\theta, \tau_{r\theta}$
$\sigma_x, \sigma_y, \tau_{xy}$ stresses in elliptic, polar and rectangular coordinates respectively, nondimensionalized with respect to σ
$K^{(m)}, K^{(b)}, K^{(tot)}$ nondimensional membrane, bending and total stress intensity factors normalized with respect to $\sigma\sqrt{a}$
q a purely imaginary parameter in the Mathieu equation, $i\beta^2h^2/2$
q_{crit} an imaginary constant, 1·46876852 i
p characteristic number of the Mathieu equation
$ce_n(\eta, q)$
$se_n(\eta, q)$ Mathieu functions of first kind
$Me_n^{(1)}(\xi, q)$
$Ne_n^{(1)}(\xi, q)$ Modified Mathieu functions of Hankel type
$J_n(z)$ Bessel function of first kind
∇^4 Square of Laplacian operator ∇^2
∇^2 $\left(\frac{\partial^2}{\partial x^2} + \frac{\partial^2}{\partial y^2}\right)$ in rectangular coordinates

$\frac{1}{K^2}\left(\frac{\partial^2}{\partial \xi^2} + \frac{\partial^2}{\partial \eta^2}\right)$ in elliptic coordinates

Superscripts: (m) and (b) denote membrane and bending components respectively.
$(\ )'$ and $(\ )^{\cdot}$ denote differentiation with respect to ξ and η respectively.

1. INTRODUCTION

In thin shell structures, like pressure vessels, high pressure ducts and aircraft fuselages, openings are invariably necessary for a variety of functional requirements like inspection, branch connections and visibility. The circular hole is generally prefered because of the advantages of its simple geometry; but, from a purely structural point of view, there are other configurations which offer certain specific advantages over the circular shape. The most important among these is the elliptical configuration. It is well known that in the case of a flat plate with an elliptic hole under a biaxial state of stress, for every stress ratio, one can find a minor axis to major axis ratio for which the stress is uniform all along the boundary. In fact, even Mansfield's neutral hole for a biaxial stress field[1] is elliptic in shape. The elliptic configuration is commonly used for window openings in aircraft fuselages and is recommended for manholes by the ASME Code for Unfired Pressure Vessels and the British Standard Specification (BS 1500) for Fusion Welded Pressure Vessels. So, in this paper we confine ourselves to the analysis of elliptic openings in cylindrical shells.

In the elliptic hole analysis, the limiting case of a crack poses itself as an important practical problem. Experimental studies in recent years have clearly shown that curvature may have considerable effect on the fatigue crack propagation rates as well as residual strength of thin-walled structures. Analysis in this paper will, therefore, be extended to straight, through cracks also. The studies will be concentrated on the evaluation of the stress intensity factors which are almost universally adopted as correlation parameters in current studies on brittle and quasi-brittle fracture of structural materials. The use of such correctly computed stress intensity factors in effectively predicting the fatigue crack growth behaviour of shells from that of flat plates with the same material and thickness has been clearly demonstrated[2, 3]

The problem of circular cutouts in thin shells has been investigated quite extensively in the past[4–9] including the problem of rigid inclusions[10] and reinforced circular cutouts [11], but the work on cutouts of noncircular shapes is not so complete. In particular, the important case of an elliptic cutout has not received sufficient attention. The first attempt on the problem of an elliptic cutout in a cylindrical shell due to Venkitapathy[12] is found to give an erroneous solution due to assumption of an inadequate solution to the governing shell equations. Perturbation solutions were obtained by Savin and Guz[13] for stresses around elliptic holes in cylindrical and spherical shells. These solutions are obtained as part of a series of investigations covering cutouts of various profiles. The method is, in principle, applicable to a cutout of any arbitrary shape provided it is possible to find a suitable mapping function which can map the contour of the hole on to a circle. The method of solution involves perturbation in two parameters β and ε defining the size and out-of-roundness of the hole. Boundary perturbation is used to reduce the problem to a series of boundary-value problems in polar coordinates, the first approximation corresponding to the problem of a circular hole. The resulting solutions are accurate enough only if the hole is small in size compared to the shell and does not depart significantly from a circle. The method has since been extended to holes of large size by Rao[11]. Here, the problem is again treated as one of perturbation in ε but, unlike in Savin and Guz's procedure, each term in the perturbation series is obtained without any restriction on the value of β by taking the solution in the form of an infinite series of Hankel functions and using a collocation procedure as in the work of Eringen et al[8]. This method, which extends applicability to large values of the curvature parameter β, places the same degree of restriction on the out-of-roundness parameter as Savin and Guz's solution and the results for a very slender ellipse would be far from being accurate. Further, it is impossible to study the limiting case of a crack by this method.

The first successful solution for the problem of an elliptic hole in a cylindrical shell without any restriction on the axis ratio k was given by Murthy[14]. The loading considered was axial tension and the major axis of the hole was taken to be parallel to shell axis. A perturbation analysis was carried out in elliptic coordinates with β as the perturbation parameter and the results are valid only if the hole is small in size compared to the shell. The analysis was later extended to the other symmetric orientation of the hole with respect to the shell and the limiting case of a crack was also analyzed[15]. The results are valid over the entire range of the parameter k and in the two limiting cases, the solutions approach known perturbation solutions for a circular hole [4] and a crack[16]. Following the techniques developed in Refs.[14, 15], the analysis has been carried further to other loading cases such as torsion[17, 18] and uniform bending moment applied along the boundary of the hole[19, 20]. Application of this method to the internal pressure loading problem

presents certain analytical difficulties and it appears impossible to obtain a closed form perturbation solution for an arbitrarily specified load transfer around the edge of the hole and, in particular, even for the usual assumption of a uniform Kirchhoff shear. On the other hand, the analysis of cracks in pressurized cylindrical shells is quite feasible and has been reported earlier by Murthy *et al.*[21].

From the foregoing review of the existing methods of analysis of elliptic holes in shells, it is evident that the earlier procedures placed restrictions on one or both of the curvature and out-of-roundness parameters β and ε. So we notice a need for a method which eliminates both these restrictions and permits analysis of practical problems. This, in fact, is the purpose of the present paper.

In the following analysis, numerical solutions are obtained for the problem of an elliptic hole and the limiting case of a crack in a circular cylindrical shell. Both the axial and transverse orientations of the hole or crack (Fig. 1) are considered with axial tension. The

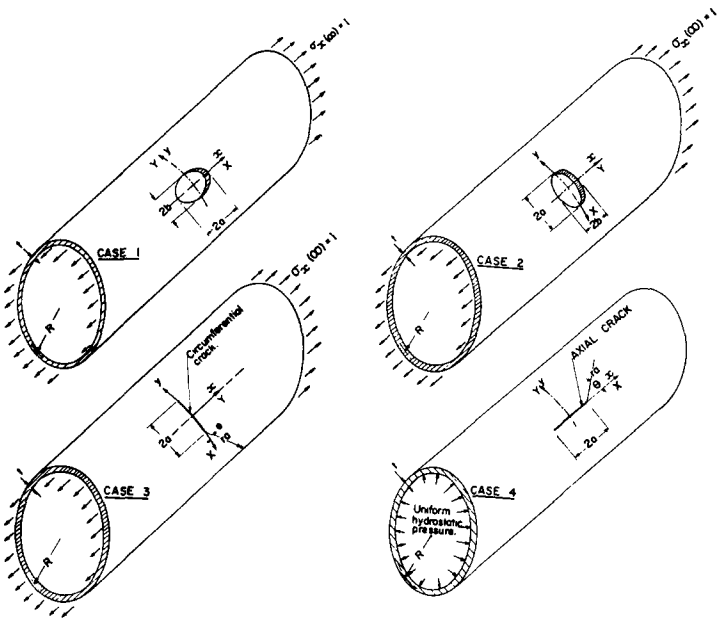

Fig. 1. Configurations considered for analysis.

axial crack is analyzed for internal pressure. The shell is considered to be thin and long enough so that end effects in the neighbourhood of the hole can be neglected. For the purpose of analysis, the shell is assumed to extend to infinity on either side of the hole. Solution to the governing differential equation for the shell is obtained in the form of an infinite series in terms of Mathieu and Modified Mathieu Functions by the method of separation of variables and is expressed in the form of a Fourier series. The boundary conditions are also formulated in the form of Fourier series and are satisfied numerically term by term with the aid of a digital computer.

The method used for solving crack problems in this paper is essentially an extension of the elliptic hole analysis, the main problem being one of recovering singular stresses from the solution in elliptic coordinates. Arbitrary constants in the series solution are evaluated by

satisfying the boundary conditions as in the elliptic hole problem with a slight modification to improve the convergence at higher values of β. The solution, which is completely determined, is then transformed by a Taylor series expansion from elliptic to polar coordinates with crack tip as the origin and the singular stresses are determined. It will be seen later that, with the Mathieu Functions and their derivatives already evaluated during earlier stages of computation, very little further computational effort is required to effect this transformation. It may be noted that whereas the problem of cracks in shells has been treated in the past exclusively by integral equation methods based on integral representations of general solutions to shell equations[16, 22–25], the present method uses the differential equation approach and is offered as an alternative to the earlier methods.

As the work reported in this paper was in progress, Tingleff[26] published a numerical solution for a transverse elliptic hole under axial tension (Fig. 1, Case 2). The analysis excluded the important limiting case of a crack and was carried out over a restricted range of β. An examination shows that this range falls below a critical value of β (which depends on k) corresponding to one of the branching points of the Mathieu equation. Solution of the problem in the neighbourhood of and beyond this critical value presents certain analytical and computational difficulties which are overcome in the present work. In fact, it is found from this analysis that at the critical value of β, the method of separation of variables fails to give an adequate solution to the shell equations and there exists another solution of variable-nonseparable type which has to be included in our solution in order to get convergence in the results. Analysis in this paper is carried through for β up to 2·5 which includes the critical values. The range of β considered here should be generally sufficient to cover sizes of openings in shells occurring commonly in practice.

2. METHOD OF ANALYSIS

2.1 *Nondimensionalization*

All the physical quantities in this paper are dimensionless and the nondimensionalizing factors are given in "Nomenclature". As a result of nondimensionalization, it is found that any given problem can be completely defined by three dimensionless parameters namely, the curvature parameter β, axis ratio k and the Poisson's ratio ν.

2.2 *System of coordinates*

In order to simplify the presentation of analysis for both orientations of the hole or crack, we define two nondimensional rectangular coordinate systems (x, y) and (X, Y) with centre of the hole as the origin. The x and X axes are oriented along the shell axis and the major axis of the hole respectively (Fig. 1). Thus

$$x = X, y = Y \quad \text{when major axis is aligned with shell axis.} \tag{1}$$

and

$$x = Y, y = -X \quad \text{when minor axis is aligned with shell axis.} \tag{2}$$

An elliptic coordinate system (ξ, η) (Fig. 2) is defined as follows:

$$X = h \cosh \xi \cos \eta, \qquad Y = h \sinh \xi \sin \eta. \tag{3}$$

The boundary of the hole is then defined by $\xi = \xi_0$ (Fig. 2). For analysis of cracks, we define nondimensional polar coordinates (r, θ) with crack tip as the origin (Fig. 1). These are related to (X, Y) by

$$X = 1 + r \cos \theta, \qquad Y = r \sin \theta. \tag{4}$$

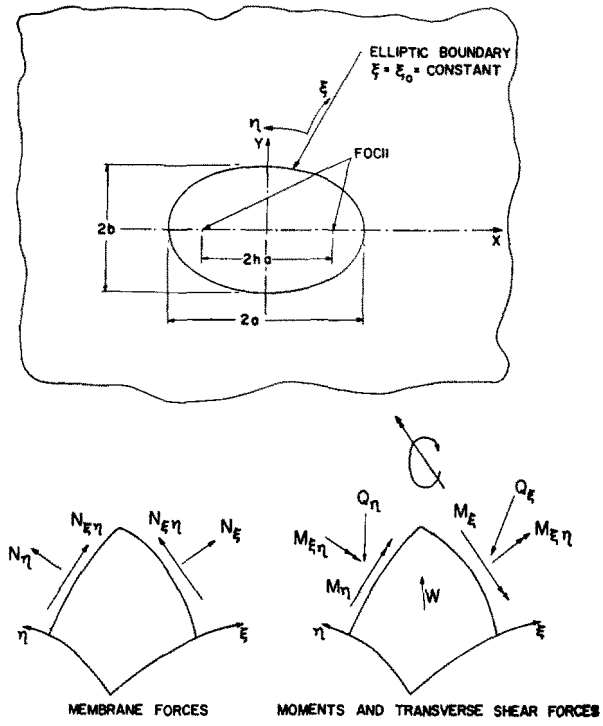

Fig. 2. System of coordinates and stress resultants.

2.3 *The "Residual problem"*

We define a "residual problem" as the problem of determining a stress field which, if superposed on the state of stress in absence of the hole, gives the actual state of stress in the shell with the hole. Evidently, this stress system should arise from a system of self-equilibrating edge loads on the hole boundary. In the problems analyzed here, these edge loads are determined from the condition that a stress-free state should exist at the boundary in the final solutions. In analysing the edge load problem, we take that part of the solution to shell equations, the stresses and displacements due to which vanish at infinity in accordance with Saint Venant's Principle.

2.4 *Governing shell equations*

For an edge load problem, Donnel's equations for a circular cylindrical shell[27] can be reduced to a single, homogeneous equation for a dimensionless complex function F:

$$\nabla^4 F + 8i\beta^2 \frac{\partial^2 F}{\partial x^2} = 0. \tag{5}$$

The nondimensional stress resultants (Fig. 2) in elliptic coordinates can be expressed in terms of F as follows:

$$N_\xi = \frac{h^2}{2K^4}\left[\Phi''(\cosh 2\xi - \cos 2\eta) + \Phi' \sinh 2\xi - \Phi \sin 2\eta\right] \tag{6}$$

$$N_\eta = \frac{h^2}{2K^4}\left[\Phi''(\cosh 2\xi - \cos 2\eta) - \Phi' \sinh 2\xi + \Phi \sin 2\eta\right] \tag{7}$$

$$N_{\xi\eta} = \frac{h^2}{2K^4}\left[\Phi'''(\cos 2\eta - \cosh 2\xi) + \Phi' \sin 2\eta + \Phi^{\cdot} \sinh 2\xi\right] \tag{8}$$

$$M_\xi = \frac{h^2}{2K^4}\left[(W'' + \nu W^{\cdot\cdot})(\cosh 2\xi - \cos 2\eta) + (1-\nu)W^{\cdot} \sin 2\eta - (1-\nu)W' \sinh 2\xi\right] \tag{9}$$

$$M_\eta = \frac{h^2}{2K^4}\left[(W^{\cdot\cdot} + \nu W'')(\cosh 2\xi - \cos 2\eta) - (1-\nu)W^{\cdot} \sin 2\eta + (1-\nu)W' \sinh 2\xi\right] \tag{10}$$

$$M_{\xi\eta} = \frac{h^2(1-\nu)}{2K^4}\left[W'^{\cdot}(\cosh 2\xi - \cos 2\eta) - W^{\cdot} \sinh 2\xi - W' \sin 2\eta\right] \tag{11}$$

$$Q_\xi = \frac{1}{K}\frac{\partial}{\partial \xi}(\nabla^2 W) \tag{12}$$

$$Q_{\dot{\eta}} = \frac{1}{K}\frac{\partial}{\partial \eta}(\nabla^2 W). \tag{13}$$

Nondimensional membrane and bending stresses can be obtained from these stress resultants by the following relations:

$$\begin{aligned} &\sigma_\xi^{(m)} = N_\xi, \qquad \sigma_\eta^{(m)} = N_\eta, \qquad \tau_{\xi\eta}^{(m)} = N_{\xi\eta}, \\ &\sigma_\xi^{(b)} = \pm 6M_\xi/\sqrt{12(1-\nu^2)}, \qquad \sigma_\eta^{(b)} = \pm 6M_\eta/\sqrt{12(1-\nu^2)} \\ &\tau_{\xi\eta}^{(b)} = \pm 6M_{\xi\eta}/\sqrt{12(1-\nu^2)}. \end{aligned} \tag{14–19}$$

The plus and minus signs in equations (17)–(19) refer to inner and outer surfaces of the shell, respectively.

2.5 *Elliptic hole with major axis parallel to shell axis* (Fig. 1, Case 1)

Solution for residual problem. In the residual problem for this case, edge loads along the hole boundary are given by

$$(N_\xi)_{\xi=\xi_0} = -\frac{1}{2}\left[1 + \frac{(\cosh 2\xi_0 \cos 2\eta - 1)}{(\cosh 2\xi_0 - \cos 2\eta)}\right] \tag{20}$$

$$(N_{\xi\eta})_{\xi=\xi_0} = \frac{1}{2}\frac{\sinh 2\xi_0 \sin 2\eta}{(\cosh 2\xi_0 - \cos 2\eta)} \tag{21}$$

$$(M_\xi)_{\xi=\xi_0} = 0 \tag{22}$$

$$(\tilde{Q}_\xi)_{\xi=\xi_0} = 0. \tag{23}$$

Where the Kirchhoff shear $\tilde{Q}_\xi$ is given by

$$\tilde{Q}_\xi = Q_\xi + \frac{1}{K}\frac{\partial M_{\xi\eta}}{\partial \eta}.$$

With the help of equations (6)–(13), the foregoing boundary conditions can be written as

$$\begin{aligned} &[\Phi^{\cdot\cdot}(\cosh 2\xi - \cos 2\eta) + \Phi' \sinh 2\xi - \Phi^{\cdot} \sin 2\eta]_{\xi=\xi_0} \\ &= -\frac{h^2}{8}(\cosh 2\xi_0 - 1)(2\cosh 2\xi_0 - 1) - \frac{h^2}{4}(\cosh 2\xi_0 - 1)^2 \cos 2\eta \\ &\quad + \frac{h^2}{8}(\cosh 2\xi_0 - 1)\cos 4\eta, \end{aligned} \tag{24}$$

$$[\Phi''(\cos 2\eta - \cosh 2\xi) + \Phi' \sin 2\eta + \Phi \sinh 2\xi]_{\xi=\xi_0} = \frac{h^2}{8} \sinh 4\xi_0 \sin 2\eta - \frac{h^2}{8} \sinh 2\xi_0 \sin 4\eta, \quad (25)$$

$$[(W'' + \nu W'')(\cosh 2\xi - \cos 2\eta) + (1 - \nu)W' \sin 2\eta - (1 - \nu)W' \sinh 2\xi]_{\xi=\xi_0} = 0, \quad (26)$$

$$\begin{aligned}[(2\cosh^2 2\xi + 1)\{W'''' + (2-\nu)W''\} - (3-\nu)W'' \sinh 4\xi \\ -2W'' \sinh 4\xi + 6W'(1-\nu) + \{6(\nu-1)W'' \cosh 2\xi \\ + 8(1-\nu)W' \sinh 2\xi\} \sin 2\eta + \{-4W'''' \cosh 2\xi \\ - 4(2-\nu)W''' \cosh 2\xi - 4(1-\nu)W' \cosh 2\xi \\ +2(3-\nu)W'' \sinh 2\xi + 4W'' \sinh 2\xi\} \cos 2\eta \\ +(3-3\nu)W'' \sin 4\eta + \{W'''' + (2-\nu)W''' \\ - 2(1-\nu)W'\} \cos 4\eta]_{\xi=\xi_0} = 0. \end{aligned} \quad (27)$$

We now seek solutions to the governing equation which fit into these boundary conditions. If G is a function satisfying the Helmholtz equation

$$\nabla^2 G + 2i\beta^2 G = 0 \quad (28)$$

it can be shown that

$$F = G \cos[(1 + i)\beta x] \quad (29)$$

and

$$F = G \sin[(1 + i)\beta x] \quad (30)$$

are solutions to equation (5). Assuming a variable-separable solution of the type

$$G = f(\xi)g(\eta) \quad (31)$$

we get

$$f'' - (p - 2q \cosh 2\xi)f = 0 \quad (32)$$

$$g'' + (p - 2q \cos 2\eta)g = 0 \quad (33)$$

where p is an arbitrary separation constant. Equations (33 and 32) can be recognized as the Mathieu and Modified Mathieu equations, respectively[28]. We can now write down the complete solution for equation (5) taking account of; (i) periodicity in η, (ii) symmetry in x and y, and (iii) the condition that stresses and displacements vanish at infinity:

$$F = \sum_{n=0,1,2,3,\ldots}^{\infty} (A_n + iB_n)F_n \quad (34)$$

where

$$F_{2j} = \cos[(1 + i)\beta x] Me_{2j}^{(1)}(\xi, q) ce_{2j}(\eta, q) \quad (35)$$

$$F_{2j+1} = \sin[(1+i)\beta x] Me_{2j+1}^{(1)}(\xi, q) ce_{2j+1}(\eta, q) \quad (36)$$

and A_n, B_n, are arbitrary real constants.

The arbitrary separation constant p in equations (32) and (33), known as the characteristic number of the Mathieu equation, is to be determined from the condition of periodicity of

the solution in η. A major difficulty in evaluating the Matheiu functions here is the determination of p for imaginary values of q. Power series expansions in q are available[28], but these extend only to a limited number of terms. Improved accuracy can be obtained by refining the approximate values from these expansions by using the procedure developed by Mulholland and Goldstein[29] based on the Newton–Raphson method. The method fails in the neighbourhood of a certain value† of $q=q_{crit}$, for which two of the characteristic numbers p_0 and p_2, corresponding to $n = 0$ and 2 in equation (34), become equal.

In the present work, the analytical procedure[28] for generating the power series for p is computerized and the series is generated without any restriction on the number of terms.‡ Over the practical range of β considered here, the series expansions are convergent for all values of n except 0 and 2. For these two values of n, the radius of convergence is equal to $|q_{crit}|$ and the convergence becomes very slow for $|q|>1$. For $|q|>1$, we use the following infinite continued fraction[28]:

$$p = \frac{-\frac{1}{2}q^2}{1-\frac{1}{4}p-}\ \frac{\frac{1}{64}q^2}{1-\frac{1}{16}p-}\ \frac{\frac{1}{576}q^2}{1-\frac{1}{36}p-}\ \frac{\frac{1}{2304}q^2}{1-\frac{1}{64}p-}\ \cdots$$

The continued fraction is truncated and expanded into a polynomial equation in p. The lowest two roots of the equation represent p_0 and p_2. The process is repeated by truncating further down till satisfactory convergence is achieved. This method works even in the neighbourhood of q_{crit} where the Newton–Raphson method fails.

Fourier series expansions are used for the Mathieu functions[28]. Two types of expansions are used in evaluating the Modified Mathieu functions, the Bessel function product series [28] being used in a major part of the computations because it is rapidly convergent. Solution to the shell equation given here represents a generalized form of the one used in circular hole problems[4–10], because the trigonometric and Hankel Functions are only degenerate forms of the Mathieu and Modified Mathieu functions. With the use of Bessel function product series, there is some difficulty in approaching the circular hole solution in the limit in a numerical analysis of this type§ and the convergence is found to be poor in a narrow band of k, $0{\cdot}9 < k \leq 1{\cdot}0$. The difficulty is overcome by using, over this restricted range of k, the other type of expansion which also involves Bessel functions but not in product form [28].

Derivatives of the Mathieu and Modified Mathieu functions are all obtained by termwise differentiation of the series, which is known to be valid[28].

Using equations (1) and (3), the trigonometric functions in equations (35) and (36) can be written in the form of Bessel–Fourier series[31]:

$$\cos[(1+i)\beta x] = J_0(v) + 2\sum_{m=1}^{\infty}(-1)^m J_{2m}(v)\cos 2m\eta \tag{37}$$

$$\sin[(1+i)\beta x] = 2\sum_{m=0}^{\infty}(-1)^m J_{2m+1}(v)\cos(2m+1)\eta \tag{38}$$

where

$$v = (1+i)\beta h\cosh\xi. \tag{39}$$

† Bouwkamp[30] gives this value to eight decimal places as $1{\cdot}46876852i$.

‡ The algebraic work, if carried out by hand, becomes increasingly formidable beyond a certain number of terms.

§ In a purely analytical work[14, 15], the limiting process is fairly simple.

From equations (37)–(39) and the Fourier series expansions for the periodic Mathieu functions $ce_n(\eta, q)$, the general term F_n in the solution given by equation (34) and its derivatives are expressed in the form of Fourier series in the η coordinate. The boundary conditions represented by equations (24)–(27) are also formulated in a similar form and are satisfied term by term in the Fourier series by considering the same number of terms, say m, in each boundary condition. In doing so, only the first $2m$ terms need be considered in the solution. This results in a system of $4m$ linear simultaneous equations for $4m$ arbitrary real constants A_n, B_n. The process is repeated for successively higher values of m until the maximum total stress remains essentially the same for a further increase in the series length.

Critical Zone of β. An interesting phenomenon was noticed during the solution of elliptic hole and crack problems in this investigation. As already mentioned, for $q=q_{crit}$, i.e. for $\beta^2(1-k^2)=2{\cdot}9375\ldots$, p_0 and p_2 become equal making the first and third terms in the series solution identical. This results in a singular solution-matrix, the first and second columns being identical to the fifth and sixth columns respectively. One might naturally think that the difficulty could be overcome by dropping one of the two identical terms in the solution. When this was done, the computations resulted in violent oscillations of stress values without any trend towards convergence.

A closer examination reveals that at $q=q_{crit}$, there exists another solution to the Helmholtz equation (28), which cannot be obtained by the method of separation of variables. By replacing one of the two identical solutions by this special solution, it is found that convergent results can be obtained at $q=q_{crit}$. Let us now see how to arrive at this solution.

If $\bar{f}(\xi)$ and $\bar{g}(\eta)$ are solutions of

$$\bar{f}'' - (p - 2q\cosh 2\xi)\bar{f} = f \tag{40}$$

$$\bar{g}'' + (p - 2q\cos 2\eta)\bar{g} = -g \tag{41}$$

where $f(\xi)$ and $g(\eta)$ satisfy equations (32) and (33), it can be easily seen that

$$G = f\bar{g} + \bar{f}g$$

is a solution of equation (28). For the existence of convergent solutions to equations (40) and (41), p must be a repeated eigen value of the Mathieu equation. Equations (40) and (41) yield series representations for $\bar{f}$ and $\bar{g}$ which are identical in form with those for f and g, i.e. $Me_n^{(1)}(\xi, q)$ and $ce_n(\eta, q)$ respectively. The difference arises only in that the characteristic coefficients in the two series satisfy a different set of recurrence relations.

For q in the neighbourhood of q_{crit}, equations (34)–(36) give an adequate solution but, as one would expect, the computations lead to large round-off errors and even loss of convergence unless they are carried out to a high degree of accuracy. In the present analysis, however, in which the calculations are extended to sixteen significant digits, convergent solutions were obtained at values of q quite close to q_{crit}.

2.6 *Elliptic hole with minor axis parallel to shell axis* (Fig. 1, Case 2)

The "residual problem" in this case is defined by the following boundary conditions:

$$(N_\xi)_{\xi=\xi_0} = -\frac{1}{2}\left[1 - \frac{(\cosh 2\xi_0 \cos 2\eta - 1)}{(\cosh 2\xi_0 - \cos 2\eta)}\right] \tag{42}$$

$$(N_{\xi\eta})_{\xi=\xi_0} = -\frac{1}{2}\frac{\sinh 2\xi_0 \sin 2\eta}{(\cosh 2\xi_0 - \cos 2\eta)} \tag{43}$$

$$(M_\xi)_{\xi=\xi_0} = 0 \tag{44}$$

$$(\tilde{Q}_\xi)_{\xi=\xi_0} = 0. \tag{45}$$

Keeping in view the changed orientation of the hole and the necessary condition of symmetry in x and y, solution to the shell equation is now taken in a slightly different form:

$$F = \sum_{n=0,1,2,3,\ldots}^{\infty} (A_n + iB_n)F_n \tag{46}$$

where

$$F_{2j} = \cos[(1+i)\beta x]Me_{2j}^{(1)}(\xi, q)ce_{2j}(\eta, q) \tag{47}$$

$$F_{2j+1} = \sin[(1+i)\beta x]Ne_{2j+1}^{(1)}(\xi, q)se_{2j+1}(\eta, q). \tag{48}$$

Since the x axis now falls along the minor axis of the hole, the trigonometric functions in equations (47) and (48) are to be expanded by using equations (2) and (3). We get

$$\cos[(1+i)\beta x] = J_0(v) + 2\sum_{m=1}^{\infty} J_{2m}(v)\cos 2m\eta \tag{49}$$

$$\sin[(1+i)\beta x] = 2\sum_{m=0}^{\infty} J_{2m+1}(v)\sin(2m+1)\eta \tag{50}$$

where

$$v = (1+i)\beta h \sinh \xi. \tag{51}$$

Beyond this point, numerical analysis of this boundary value problem follows essentially the same pattern as in Section 2.5.

As crack is one of the limiting cases of the ellipse, we now proceed to extend the analysis of Sections 2.5 and 2.6 to the study of cracks in cylindrical shells. The axial crack is trivial for axial tension and so will be examined later for internal pressure. The circumferential crack is an important case for axial tension loading and will be examined in the next section.

2.7 *Circumferential crack* (*Fig.* 1, *Case* 3)

As this problem is a limiting case of the transverse elliptic hole (Fig. 1, Case 2), all the relations developed in Section 2.6, including the boundary conditions, are valid. The arbitrary constants in the series solution are determined by satisfying the boundary conditions given by equations (42)–(45) term by term in the Fourier series as in the elliptic hole problem. It should be emphasized here that although we have singular stresses at the crack tip, we are not trying to expand any singular function as a Fourier series in satisfying the boundary conditions. Let us, for example, take the boundary condition

$$N_{\xi\eta} = \frac{h^2}{2K^4}[\Phi'''(\cos 2\eta - \cosh 2\xi) + \Phi' \sin 2\eta + \Phi \sinh 2\xi] = 0 \quad \text{at} \quad \xi = 0. \tag{52}$$

$N_{\xi\eta}$, in general, is singular at the crack tip as K is zero at this point on the boundary. While actually satisfying the foregoing boundary condition, we take it in the form

$$[\Phi'''(\cos 2\eta - \cosh 2\xi) + \Phi' \sin 2\eta + \Phi \sinh 2\xi]_{\xi=0} = 0. \tag{53}$$

The left hand side of equation (53), as it follows from the well known properties of the Mathieu and Modified Mathieu functions, is not singular anywhere over the domain considered. It is this we are expanding in a Fourier series and making it vanish term by term.

With the arbitrary constants determined, the solution is completely known in elliptic coordinates. However, it is convenient to express crack solutions in terms of polar coordinates with crack tip as the origin because, in this form, the order and strength of singularity of stresses can be clearly seen. Hence, we transform the solution to polar coordinates and recover the singular stresses in the usual form. Since we are only interested in determining the singular stresses near the crack tip, these transformations are carried out for

$$r \ll 1. \tag{54}$$

Terms involving r^2 and higher powers of r are neglected in F because they produce only finite stresses. Accordingly, the trigonometric functions in equations (47) and (48) are expanded with the help of equations (2) and (4), as

$$\cos[(1+i)\beta x] = 1 + 0(r^2) \tag{55}$$

$$\sin[(1+i)\beta x] = (1+i)\beta r \sin\theta + 0(r^3). \tag{56}$$

Without any loss of generality, we can restrict ourselves to one of the crack tips where $\eta = 0$ as the stress system is symmetric about X and Y axes. Since $\xi = 0$ on the crack boundary, we have, in the vicinity of this crack tip,

$$\xi \ll 1, \qquad \eta \ll 1. \tag{57}$$

Making use of (54), (57) and equations (3) and (4), the following relations between the elliptic and polar coordinates are obtained;

$$\xi = (2r)^{1/2} \cos\frac{\theta}{2} - \frac{1}{6\sqrt{2}} r^{3/2} \cos\frac{3\theta}{2} + 0(r^2) \tag{58}$$

$$\eta = (2r)^{1/2} \sin\frac{\theta}{2} - \frac{1}{6\sqrt{2}} r^{3/2} \sin\frac{3\theta}{2} + 0(r^2). \tag{59}$$

In view of (57), Taylor series expansions for the Mathieu and Modified Mathieu functions in the neighbourhood of the crack tip are written as

$$ce_n(\eta, q) = ce_n(0, q) + \frac{\eta}{\lfloor 1} ce_n'(0, q) + \frac{\eta^2}{\lfloor 2} ce_n''(0, q) + \frac{\eta^3}{\lfloor 3} ce_n'''(0, q) + 0(\eta^4) \tag{60}$$

$$se_n(\eta, q) = se_n(0, q) + \frac{\eta}{\lfloor 1} se_n'(0, q) + \frac{\eta^2}{\lfloor 2} se_n''(0, q) + \frac{\eta^3}{\lfloor 3} se_n'''(0, q) + 0(\eta^4) \tag{61}$$

$$Me_n(\xi, q) = Me_n(0, q) + \frac{\xi}{\lfloor 1} Me_n'(0, q) + \frac{\xi^2}{\lfloor 2} Me_n''(0, q) + \frac{\xi^3}{\lfloor 3} Me_n'''(0, q) + 0(\xi^4) \tag{62}$$

$$Ne_n(\xi, q) = Ne_n(0, q) + \frac{\xi}{\lfloor 1} Ne_n'(0, q) + \frac{\xi^2}{\lfloor 2} Ne_n''(0, q) + \frac{\xi^3}{\lfloor 3} Ne_n'''(0, q) + 0(\xi^4). \tag{63}$$

Superscript (1) is omitted in $Me_n(\xi, q)$ and $Ne_n(\xi, q)$ for the sake of brevity. Terms involving fourth and higher powers of ξ and η are dropped in the series as ξ and η are of order $r^{1/2}$. From the Fourier series expansions for Matheiu functions, there follows

$$ce_n'(0, q) = ce_n'''(0, q) = se_n(0, q) = se_n''(0, q) = 0. \tag{64}$$

From the properties of Mathieu and Modified Mathieu functions, it can be shown that

$$Me_n(0, q)ce_n''(0, q) + Me_n''(0, q)ce_n(0, q) = 0. \tag{65}$$

Using equations (55, 56 and 58–65), the general term in the series solution defined by equations (47) and (48) can be expressed in terms of polar coordinates as follows:

$$\begin{aligned} F_{2j} = {} & Me_{2j}(0, q)ce_{2j}(0, q) + \sqrt{2}Me'_{2j}(0, q)ce_{2j}(0, q)r^{1/2}\cos\frac{\theta}{2} + Me''_{2j}(0, q)ce_{2j}(0, q)r\cos\theta \\ & + \frac{1}{2\sqrt{2}}[Me'''_{2j}(0, q)ce_{2j}(0, q) + Me'_{2j}(0, q)ce''_{2j}(0, q)]r^{3/2}\cos\frac{\theta}{2} \\ & + \left[\frac{\{Me'''_{2j}(0, q) - Me'_{2j}(0, q)\}ce_{2j}(0, q)}{6\sqrt{2}} - \frac{Me'_{2j}(0, q)ce''_{2j}(0, q)}{2\sqrt{2}}\right]r^{3/2}\cos\frac{3\theta}{2} + 0(r^2) \end{aligned} \tag{66}$$

$$F_{2j+1} = \frac{(1 + i)\beta}{\sqrt{2}}Ne_{2j+1}(0, q)se'(0, q)r^{3/2}\left(\cos\frac{\theta}{2} - \cos\frac{3\theta}{2}\right) + 0(r^2). \tag{67}$$

Determination F_{2j} and F_{2j+1} from the foregoing equations is fairly simple from the computational points of view, because the Modified Mathieu functions and their first, second and third derivatives on the crack boundary $\xi = 0$ are already evaluated during the process of satisfying the boundary conditions. Mathieu functions and their derivatives at $\eta = 0$ are easily determined from their Fourier series expansions. Solution for F in polar coordinates is obtained by substituting for F_{2j} and F_{2j+1} and carrying out the summation in equation (46). Separating the real and imaginary parts, we get the stress function and normal displacement in the form

$$\Phi = \Phi_0 + \Phi_1 r^{1/2}\cos\frac{\theta}{2} + \Phi_2 r\cos\theta + \Phi_3 r^{3/2}\cos\frac{\theta}{2} + \Phi_4 r^{3/2}\cos\frac{3\theta}{2} + 0(r^2) \tag{68}$$

$$W = W_0 + W_1 r^{1/2}\cos\frac{\theta}{2} + W_2 r\cos\theta + W_3 r^{3/2}\cos\frac{\theta}{2} + W_4 r^{3/2}\cos\frac{3\theta}{2} + 0(r^2). \tag{69}$$

Nondimensional stresses and stress resultants can be determined from the known solution by using the relations

$$N_r = \sigma_r^{(m)} = \frac{1}{r}\frac{\partial\Phi}{\partial r} + \frac{1}{r^2}\frac{\partial^2\Phi}{\partial\theta^2} \tag{70}$$

$$N_\theta = \sigma_\theta^{(m)} = \frac{\partial^2\Phi}{\partial r^2} \tag{71}$$

$$N_{r\theta} = \tau_{r\theta}^{(m)} = -\frac{\partial}{\partial r}\left(\frac{1}{r}\frac{\partial\Phi}{\partial\theta}\right). \tag{72}$$

$$M_r = -[12(1 - \nu^2)]^{1/2}\sigma_r^{(b)}/6 = \frac{\partial^2 W}{\partial r^2} + \nu\left(\frac{1}{r}\frac{\partial W}{\partial r} + \frac{1}{r^2}\frac{\partial^2 W}{\partial\theta^2}\right) \tag{73}$$

$$M_\theta = -[12(1 - \nu^2)]^{1/2}\sigma_\theta^{(b)}/6 = \nu\frac{\partial^2 W}{\partial r^2} + \frac{1}{r}\frac{\partial W}{\partial r} + \frac{1}{r^2}\frac{\partial^2 W}{\partial\theta^2} \tag{74}$$

$$M_{r\theta} = -[12(1-\nu^2)]^{1/2}\tau_{r\theta}^{(b)}/6 = (1-\nu)\frac{\partial}{\partial r}\left(\frac{1}{r}\frac{\partial W}{\partial \theta}\right) \tag{75}$$

$$Q_r = \frac{\partial}{\partial r}(\nabla^2 W) \tag{76}$$

$$Q_\theta = \frac{1}{r}\frac{\partial}{\partial \theta}(\nabla^2 W) \tag{77}$$

where the bending stresses refer to outer surface of the shell.

A simple check on the computed values of Φ_n and W_n in equations (68) and (69) is to check whether the following boundary conditions, reformulated in polar coordinates, are satisfied or not:

$$N_\theta = -1,\ N_{r\theta} = M_\theta = \tilde{Q}_\theta = 0 \quad \text{along} \quad \theta = \pm\pi$$

where

$$\tilde{Q}_\theta = Q_\theta + \frac{\partial M_{r\theta}}{\partial \theta}$$

Substituting from equations (68)–(77) in the foregoing boundary conditions and satisfying the resulting equations term by term in the power series in $r^{1/2}$, there follows

$$\Phi_1 = 0 \tag{78}$$

$$W_1 = 0 \tag{79}$$

$$\Phi_3/\Phi_4 = 3 \tag{80}$$

$$W_3/W_4 = 3(\nu-1)/(7+\nu). \tag{81}$$

The constant terms and terms involving $r\cos\theta$ in equations (68) and (69) do not produce any stress. In view of this and also from equations (78) and (79), it is evident that the membrane and bending stresses have the same $1/\sqrt{r}$ type of singularity characteristic of plates. Hence, following the plate convention, we define the membrane and bending stress intensity factors $K^{(m)}$ and $K^{(b)}$ with reference to the cleavage plane stress:

$$[\sigma_\theta^{(m)}]_{\theta=0} = K^{(m)}/\sqrt{2r} + 0(r^0) \tag{82}$$

$$[\sigma_\theta^{(b)}]_{\theta=0} = K^{(b)}/\sqrt{2r} + 0(r^0) \tag{83}$$

where the bending stress refers to the outer surface of the shell. An inspection shows that $K^{(m)}$ and $K^{(b)}$ are dimensionless and are normalized with respect to $\sigma\sqrt{a}$ which represents the stress intensity factor for an infinite plate. From equations (82, 83 and 68–75), the membrane and bending stress intensity factors are obtained as simple algebraic expressions involving Φ_3, Φ_4, W_3 and W_4.

$$K^{(m)} = 3(\Phi_3 + \Phi_4)/2\sqrt{2} \tag{84}$$

$$K^{(b)} = 3[3W_4(1-\nu) - W_3(5+3\nu)]/[24(1-\nu^2)]^{1/2}. \tag{85}$$

Distribution of stresses in the vicinity of the crack tip is obtained in terms of $K^{(m)}$ and $K^{(b)}$ through equations (70–75, 68, 69, 78–83), used in that order:

Membrane stresses

$$\sigma_X^{(m)} = \frac{K^{(m)}}{\sqrt{2r}}\left[\tfrac{3}{4}\cos\frac{\theta}{2} + \tfrac{1}{4}\cos\frac{5\theta}{2}\right] + 0(r^0) \tag{86}$$

$$\sigma_Y^{(m)} = \frac{K^{(m)}}{\sqrt{2r}}\left[\tfrac{5}{4}\cos\frac{\theta}{2} - \tfrac{1}{4}\cos\frac{5\theta}{2}\right] + 0(r^0) \tag{87}$$

$$\tau_{XY}^{(m)} = \frac{K^{(m)}}{\sqrt{2r}}\left[\tfrac{1}{4}\sin\frac{5\theta}{2} - \tfrac{1}{4}\sin\frac{\theta}{2}\right] + 0(r^0). \tag{88}$$

Bending Stresses (Outer Surface)

$$\sigma_X^{(b)} = \frac{K^{(b)}}{(3+\nu)\sqrt{2r}}\left[-\frac{3(1-\nu)}{4}\cos\frac{\theta}{2} - \frac{(1-\nu)}{4}\cos\frac{5\theta}{2}\right] + O(r^0) \tag{89}$$

$$\sigma_Y^{(b)} = \frac{K^{(b)}}{(3+\nu)\sqrt{2r}}\left[\frac{(11+5\nu)}{4}\cos\frac{\theta}{2} + \frac{(1-\nu)}{4}\cos\frac{5\theta}{2}\right] + O(r^0) \tag{90}$$

$$\tau_{XY}^{(b)} = \frac{K^{(b)}}{(3+\nu)\sqrt{2r}}\left[-\frac{(7+\nu)}{4}\sin\frac{\theta}{2} - \frac{(1-\nu)}{4}\sin\frac{5\theta}{2}\right] + O(r^0). \tag{91}$$

The test of convergence during computations was applied on the total stress intensity factor $K^{(tot)}$ which is given by

$$K^{(tot)} = K^{(m)} + K^{(b)}$$

and which represents the physically most significant quantity in the crack problem. The results showed satisfactory convergence for β up to 1·25 whereas, for higher values of β, there was no convergence at all. Let us now examine the reason for this and see what modifications would be necessary in our procedure for $\beta > 1{\cdot}25$.

Taking, for instance, the boundary condition (52) and its equivalent, equation (53), we see that $N_{\xi\eta}$ is actually obtained by dividing the left hand side of equation (53) by $2K^4/h^2$. While K is a mathematically perfect zero at the crack tip, the left hand side of equation (53) leaves a residue due to round-off errors in the computer. The magnitude of this residue, as would be expected, increases with β and the result is that we have residual traction forces of singular nature in the vicinity of the crack tip. This accounts for poor convergence at higher values of β. We thus find that the Fourier series technique, in spite of its proven effectiveness in satisfying the overall boundary conditions, cannot handle the mathematical limiting process in the vicinity of the crack tip for higher values of β.

We now look back at equations (78)–(81) which are obtained by reformulating the boundary conditions in polar coordinates. These equations serve as a useful check on the mathematical formulation of the problem, the correctness of computer programming as well as computational errors such as round-off, etc. Numerical results show that, for $\beta \leq 1{\cdot}25$ these equations are clearly satisfied and convergence is found in the results. For $\beta > 1{\cdot}25$, equations (78)–(81) are not satisfied and convergence is not achieved. So one concludes that there is no error either in the mathematical formulation or in the computer programming, but the numerical errors are overpowering the solution at higher values of β. The value of β beyond which this happens is obviously not unique but depends on the computer limitations and the programming detail.

A closer look at the origin of equations (78)–(81) shows that they actually represent boundary conditions on the singular component of stresses near the crack tip. A remedy for the difficulty in achieving convergence at $\beta > 1{\cdot}25$ now becomes immediately obvious. Since equations (78)–(81), after all, represent the boundary conditions in some form, these can be enforced as additional conditions to be satisfied during the evaluation of the arbitrary constants. What we are doing is, in effect, equivalent to (i) satisfying the overall boundary conditions by enforcing them term by term in the Fourier series, and (ii) taking particular care of the singular stresses in the boundary conditions through equations (78)–(81). This "hybrid" technique of satisfying the boundary conditions results in excellent convergence. over the entire range of β considered here. For $\beta \leq 1{\cdot}25$, however, it makes no difference whether the Fourier series method is used alone or in conjunction with equations (78)–(81).

2.8 *Axial crack* (Fig. 1, Case 4)

In the "residual problem" for a pressurized cylindrical shell with an axial crack, the edge loads along the crack are

$$N_\xi = -1,\ N_{\xi\eta} = M_\xi = \tilde{Q}_\xi = 0 \quad \text{along} \quad \xi = 0.$$

The axial crack being a limiting case of an elliptic hole with major axis parallel to shell axis, the solution to the shell equation is taken as in equations (34)–(36). From equations (1, 4 and 54), it follows that

$$\cos[(1+i)\beta x] = \cos[(1+i)\beta] - (1+i)\beta \sin[(1+i)\beta] r\cos\theta + 0(r^2) \tag{92}$$

$$\sin[(1+i)\beta x] = \sin[(1+i)\beta] + (1+i)\beta \cos[(1+i)\beta] r\cos\theta + 0(r^2). \tag{93}$$

Using equations (92, 93 and 58–65), the general term in the series solution defined by equations (35) and (36) can be expressed in polar coordinates as follows:

$$\begin{aligned} F_n = {} & \lambda Me_n(0,q)ce_n(0,q) + \sqrt{2}\lambda Me_n'(0,q)ce_n(0,q) r^{1/2}\cos\frac{\theta}{2} \\ & + [\lambda Me_n''(0,q)ce_n(0,q) + (1+i)\beta\mu Me_n(0,q)ce_n(0,q)] r\cos\theta \\ & + \left[\frac{\lambda}{2\sqrt{2}}\{Me_n'''(0,q)ce_n(0,q) + Me_n'(0,q)ce_n''(0,q)\}\right. \\ & \left. + \frac{(1+i)\beta\mu}{\sqrt{2}} Me_n'(0,q)ce_n(0,q)\right] r^{3/2}\cos\frac{\theta}{2} \\ & + \left[\frac{\lambda\{Me_n'''(0,q) - Me_n'(0,q)\}ce_n(0,q)}{6\sqrt{2}} - \frac{\lambda Me_n'(0,q)ce_n''(0,q)}{2\sqrt{2}}\right. \\ & \left. + \frac{(1+i)\beta\mu}{\sqrt{2}} Me_n'(0,q)ce_n(0,q)\right] r^{3/2}\cos\frac{3\theta}{2} + O(r^2) \end{aligned}$$

where

$$\lambda = \cos[(1+i)\beta], \quad \mu = -\sin[(1+i)\beta] \quad \text{for } n \text{ even}$$

$$\lambda = \sin[(1+i)\beta], \quad \mu = \cos[(1+i)\beta] \quad \text{for } n \text{ odd}.$$

Further analysis of this problem is carried out essentially on the same lines as in the circumferential crack case. In fact, all the relations given by equations (68)–(91), without modifications, hold good for this case also.

The direct use of the Fourier series method, without inclusion of equations (78)–(81), in satisfying the boundary conditions proved successful for β up to 1·5 which is slightly higher than the corresponding limit for a circumferential crack. As it was desired to go beyond this limit up to $\beta = 2{\cdot}5$, equations (78)–(81) arising from the power series expansions of the boundary conditions along the crack were used together with the Fourier series expansions in η.

3. RESULTS AND DISCUSSION

Numerical calculations in this paper were performed on an IBM 360/44 computer. Results are obtained, for Poisson's ratio of 0·3, in terms of the two dimensionless parameters β and k in the ranges

$$0 < \beta \leq 2{\cdot}5 \quad \text{and} \quad 0 \leq k \leq 1.$$

For each value of β and k, the computation was started by taking the first ten terms in the series solution initially and increasing the number of terms in steps of two. Computations were terminated if less than 0·1 per cent deviation was noticed in stresses from two successive approximations. Over the range of β covered here, it was generally found sufficient to consider the first twelve terms.

Perturbation solutions are available [14–16, 21, 22] for all the problems for which numerical results are given here. As would be anticipated, comparison of perturbation solutions with the present accurate results show good agreement for small values of β (up to 0·25). In fact, for very small values of β (say, $\beta = 0{\cdot}005$) the results agree up to four significant digits in stresses as well as in the arbitrary constants. Such a comparison provides a useful check against errors in programming our method over the digital computer and also confirms the effectiveness of the perturbation method for small β. The accuracy of perturbation solutions beyond $\beta = 0{\cdot}25$ is found to differ slightly from one problem to an other. An example of the increasing discrepancy for higher values of β can be seen in Fig. 3.

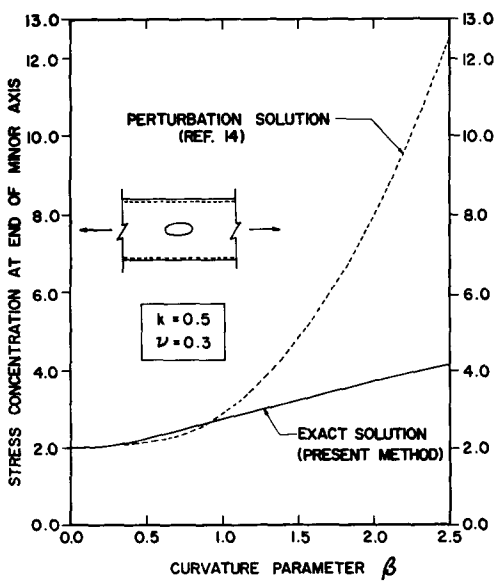

Fig. 3. Comparison of perturbation and exact solutions.

In view of the range of problems covered in this analysis, only important results like stress concentration factors for elliptic holes and nondimensional stress intensity factors for cracks are presented. Parametric studies are presented only for a longitudinal elliptic hole (Fig. 1, Case 1) but the conclusions are generally valid for the transverse elliptic hole also.

Results for an elliptic hole with major axis parallel to shell axis for the axial loading case are shown in Figs. 3–7. Figures 4 and 5 show the variation of stresses on the hole boundary

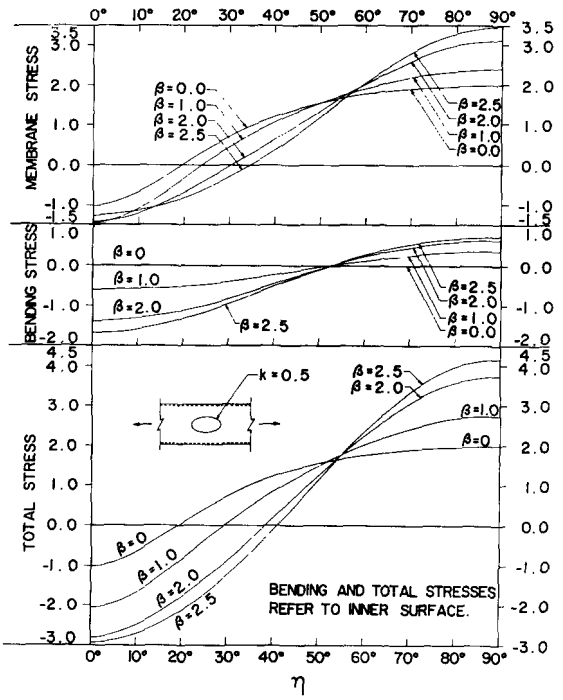

Fig. 4. Stresses along the hole boundary plotted as a function of β.

in terms of β and k. It can be seen that the peak value of membrane stress in tension is always reached at the ends of minor axis and its magnitude increases with β and the axis ratio k. The maximum value of membrane stress in compression, however, increases with β, up to a certain limit and decreases with further increase in β, as in a circular hole[9]. Further, for higher values of β, its location drifts away from the end of major axis as the ellipse approaches a circle as can be seen from Fig. 5 plotted for $\beta = 2{\cdot}0$. A similar phenomenon can be noticed in the circular hole solutions reported earlier[9]. The bending stress increases with increase in β and k everywhere on the boundary, the maximum being always reached at the ends of major axis for any given β and k. With increase in β, the bending stress becomes quite significant. In fact, for a 2:1 elliptic hole with $\beta = 2{\cdot}5$, the maximum bending stress is as large as 1·69 times the applied stress at infinity and is even greater than the membrane stress at the same point (Fig. 4).

The effect of curvature parameter on the decay of membrane and bending components of the axial stress in the circumferential direction is shown in Fig. 6. It can be observed that stresses at the hole boundary increase in magnitude with increase in β, but they decay much faster also, as would be anticipated from the asymptotic expansion of the solution to shell

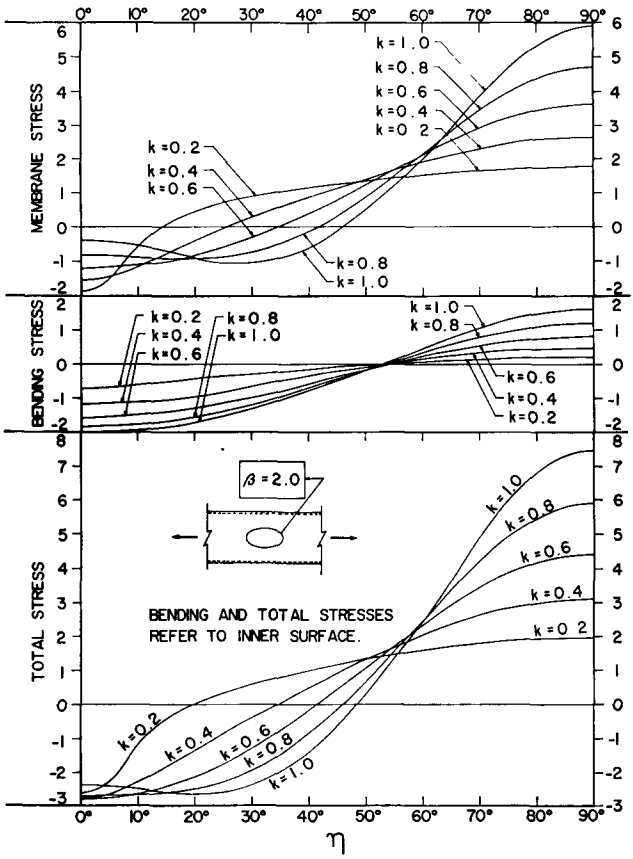

Fig. 5. Stresses along the hole boundary plotted as a function of k.

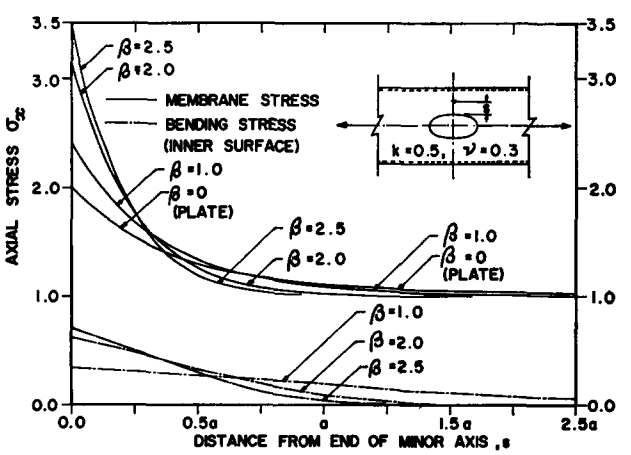

Fig. 6. Decay of stresses in the hoop direction.

equation[14]. Numerical results show that the rate of decay varies with the direction, being slowest and most rapid in the axial and circumferential directions respectively.

Wall bending takes place in such a way that, in highly stressed regions on the boundary, the bending stress has the same sign as the membrane stress on the inner surface of the shell as seen from Figs. 4 and 5. Thus, for a longitudinal elliptical hole (Fig. 1, Case 1), the maximum total stress always occurs at the ends of minor axis and on the inner surface. Figure 7

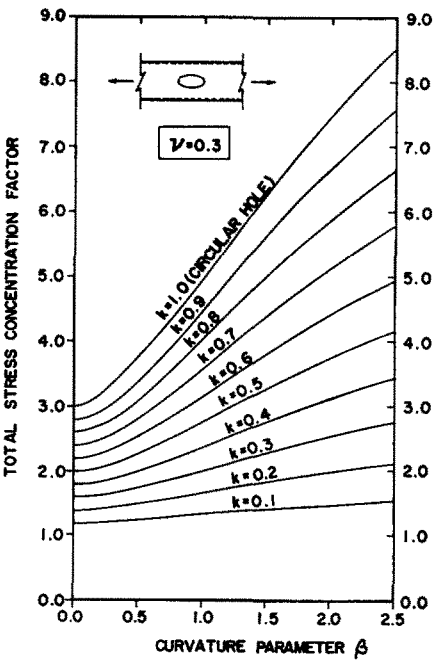

Fig. 7. Stress concentration factor for an elliptic hole with major axis parallel to shell axis.

shows a plot of the stress concentration factor based on this maximum total stress against β for various values of k at intervals of 0·1. Similar results for an elliptic hole with minor axis parallel to shell axis are given in Fig. 8. In this case, the maximum total stress occurs at the ends of major axis and on the inner surface.

For the limiting case of a circumferential crack, the membrane and bending stress intensity factors are given by Figs. 9 and 10. The corresponding results for an axial crack under pressure loading are shown in Figs. 11 and 12. There are several interesting features common to both the axial and circumferential crack problems:

(i) For small values of β, the variation of membrane stress intensity factor is parabolic and the numerical results agree with the following perturbation results given by Folias [16, 22] and Murthy *et al.*[15, 21].

$$K^{(m)} = 1 + \frac{\pi\beta^2}{8} \qquad \text{for a circumferential crack}$$

$$K^{(m)} = 1 + \frac{5\pi\beta^2}{8} \qquad \text{for an axial crack.}$$

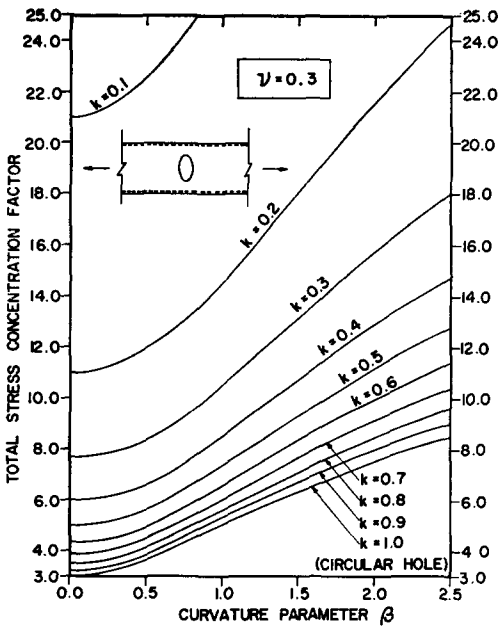

Fig. 8. Stress concentration factor for an elliptic hole with minor axis parallel to shell axis.

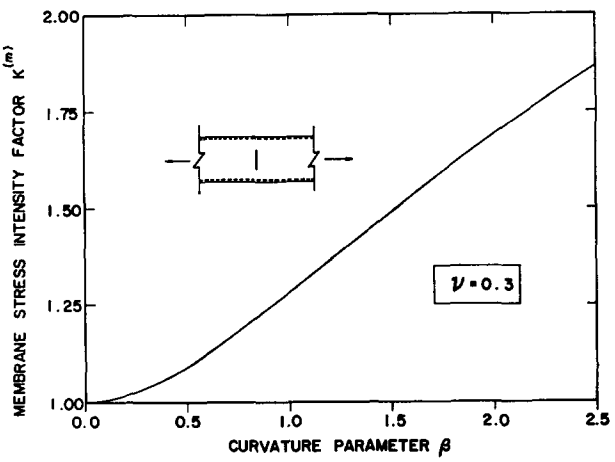

Fig. 9. Membrane stress intensity factor for a circumferential crack.

For higher values of β, it can be seen from Figs. 9 and 11 that the variation of $K^{(m)}$ is approximately linear. In fact, for an axial crack, the curve is almost indistinguishable from a straight line. The following relations, obtained from a least square fit, can be used to give a good approximation for $0{\cdot}5 \leq \beta \leq 2{\cdot}5$ with less than one per cent error;

$$K^{(m)} = 0{\cdot}392\beta + 0{\cdot}897 \quad \text{for} \quad \text{a circumferential crack}$$
$$K^{(m)} = 1{\cdot}36\beta + 0{\cdot}662 \quad \text{for} \quad \text{an axial crack.}$$

(ii) The bending stress intensity factor $K^{(b)}$ increases with β up to a certain limit, reaches a positive maximum and decreases with further increase in β. Later, it changes sign and the negative value increases in magnitude continuously in the range considered.

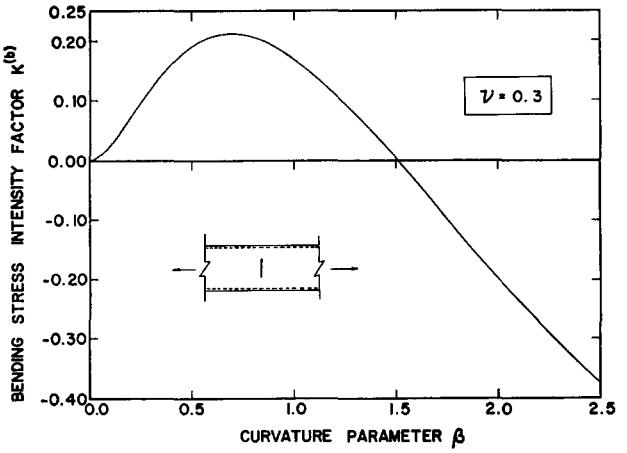

Fig. 10. Bending stress intensity factor for a circumferential crack.

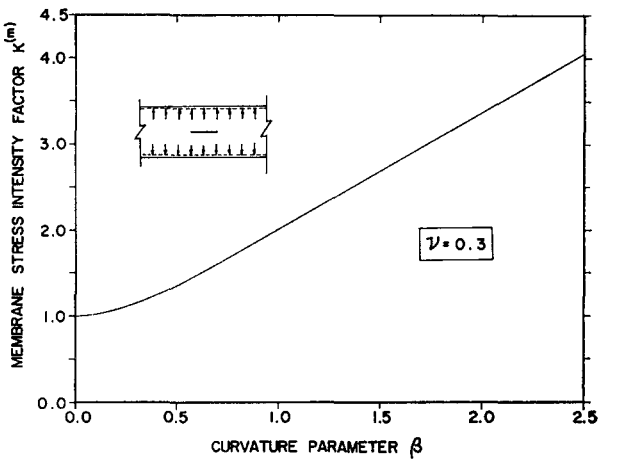

Fig. 11. Membrane stress intensity factor for an axial crack.

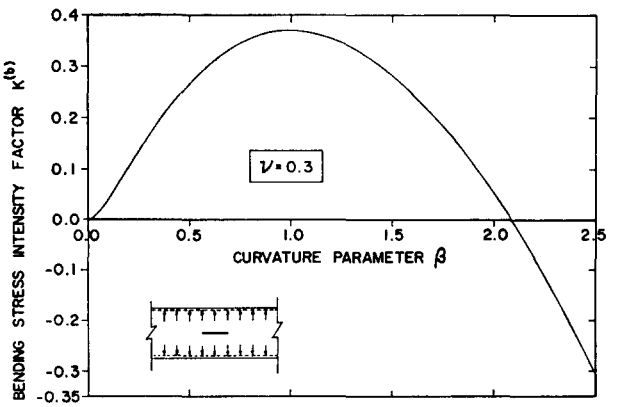

Fig. 12. Bending stress intensity factor for an axial crack.

These trends in the behaviour of $K^{(m)}$ and $K^{(b)}$ are also seen in the earlier works of Copley and Sanders[23] and Erdogan and Ratwani[25] which are based on integral equation methods.

(iii) The distribution patterns of the membrane and bending stresses in the vicinity of the crack tip, given by equations (86)–(91) are identical with those encountered in plate problems for the cases of stretching[32] and bending[33], both with regard to the inverse square root singularity in r and angular distribution in the θ coordinate. This, of course, is a consequence of the use of Kirchhoff shear in the boundary conditions. While curvature leaves the radial and angular distribution of stresses unaltered, it has the effect of increasing their amplitude. This effect is more predominant in the case of an axial crack. For instance, for $\beta = 2{\cdot}5$, the total stress intensity factor for circumferential and axial cracks are 2·23 and 4·36, respectively. This shows that curvature in a plane perpendicular to the crack is more critical from a stress point of view.

Equations (86)–(91) suggest that the angular distribution of membrane stresses is independent of the Poisson's ratio whereas this is not true of bending stresses. Analysis of the plate bending problem from Reissner's theory by Knowles and Wang[34] shows that the order of singularity of bending stresses near the crack tip agrees with predictions from Kirchhoff theory [33] but the angular distribution is independent of ν and is exactly identical with one for the case of pure stretching[32]. Pending a similar investigation of the shell problem, it might be expected that the same conclusion should hold good for shells also.

Results given here cannot be directly compared with some of the other theoretical solutions due to assumption of different values of Poisson's ratio. Wherever necessary, separate computations were carried out for making such comparisons and the results are found to be in agreement with those given in Refs.[9, 23 and 26]. Comparisons could not be made with the work of Erdogan and Ratwani[25] as the value of ν used in their computations is not clear.

The authors could not find sufficient experimental data to compare results from the present method of analysis with those obtained by experiments. The only extensive series of tests on elliptic holes in shells due to Leckie *et al.*[35] is restricted to pressurized spherical shells. In a series of photoelastic tests on shells with cutouts reported by Houghton[36], only one cylindrical shell model with an elliptic hole was tested for the case of axial tension. Transmission polariscope was used and the polariser was set inside the cylinder with the hole under examination between it and the analyzer. By this arrangement, stresses in the far wall of the cylinder did not interfere with those being measured. The hole was relatively small in size with a β value of 0·6 and it appears that experimental errors were more predominant than the effect of curvature. This is evidenced by the fact that the maximum direct stress on the hole boundary was found to be less than that in a plate, whereas it has been established beyond doubt by theoretical as well as experimental investigations that curvature has the effect of increasing the maximum direct stress. However, comparison with limited results from the work of Hasseem *et al*[37] shows good agreement between experiment and results from the present theoretical method as seen in Fig. 13. Here again, as part of a general series of photoelastic investigations on cutouts in cylindrical as well as conical shells, only one model with a transverse elliptic hole was tested under axial tension (Fig. 1, Case 2). Details of the model tested are

$$R = 3'', \qquad t = 0{\cdot}09'', \qquad a = 1'', \qquad b = 0{\cdot}5''$$

and $\nu = 0{\cdot}5$ (corresponding to the condition at stress freezing). The model thus had a β

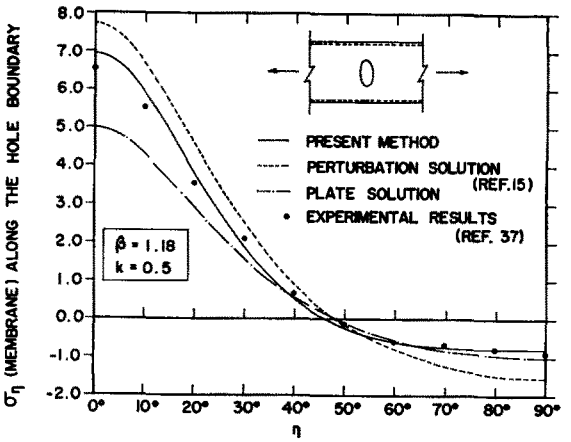

Fig. 13. Comparison with experimental results.

value of 1·18. The load was applied at the critical temperature and the model was stress frozen. The inner face around the cutout in the stress frozen model was given a thin aluminium spray coating to provide a reflective surface and reflection polariscope was used. Hence only direct stresses could be measured.

Computations throughout the paper are carried out for $\nu = 0{\cdot}3$ which nearly represents the value for most of the engineering materials. Effect of varying Poisson's ratio for a given β has been investigated for the analogous problems of a circular hole[8] and an axial crack[38]. It is found that there is a slight increase in stress concentration factor or the stress intensity factor, as the case may be, but this is compensated by the fact that β itself is a decreasing function of ν. A more realistic picture emerges by varying ν for a given $a/\sqrt{Rt}$. Such an analysis[38] shows that the influence of Poisson's ratio is negligible.

3.1 *Application of results to residual strength evaluation*

The elastic stress intensity factor has been successfully used for brittle and quasi-brittle materials as a correlation parameter in evaluating residual strengths of cracked structures. In other words, for such a material, there exists a critical value of the elastic stress intensity factor at which fracture takes place. In the case of moderately large plastic deformations characteristic of ductile materials, correlations based on the use of elastic stress intensity factor as a direct correlation parameter are rather poor. This deficiency has been partly remedied in the past for the plate problem by introducing a correction due to plasticity effects to the elastic stress intensity factor[39–41]. In particular, the plastic strip model introduced by Dugdale[40] appears to be fairly realistic and seems to agree with the available experimental results. Dugdale's model has been recently modified for shell problems[42] to take account of the combined effect of stretching and bending. An analysis[38] of the result of a series of burst tests obtained by Anderson and Sullivan[43] on 2014–T6 aluminium cylinders shows that the plasticity corrected stress intensity factor computed in this way is a fairly accurate means of predicting the residual strength except in the case of very small crack lengths. In recent years, however, the COD (Crack Opening Displacement) Theory is being widely recognized as a fracture criterion[44, 45], particularly in the United Kingdom. The theory is based on the assumption that the unstable crack growth occurs when the

COD, defined as the relative crack opening at the actual crack tip obtained from the plastic strip model, reaches a critical value.

It should however be emphasized at this point that for determining either the plasticity corrected stress intensity factor or the COD, results of an elastic analysis of the type reported in this paper form a prerequisite.

3.2 *Application to fatigue crack propogation studies*

In applying conventional crack propogation theories to shell problems characterized by the combined action of stretching and bending, it has been suggested[38] that an effective stress intensity factor ratio K_{eff} given by

$$K_{eff}=K^{(m)}+\tfrac{1}{2}K^{(b)} \tag{94}$$

should be used. Some justification for this based on an extension of Dugdale's plastic strip model to cylindrical bending in plates is given in Ref.[46]. This has also been substantiated by Erdogan and Ratwani[38] by fatigue tests on plate and shell specimens of the same material (6061-T4 aluminium). Results of these tests show that with the use of stress intensity factor ratio given by equation (94) and the material constants determined through tests on plate specimens, it is possible to predict the fatigue crack growth behaviour of shells of the same material and thickness.

4. CONCLUDING REMARKS

The paper gives an account of a fairly extensive numerical work on the stress problem of large sized elliptic holes and cracks in cylindrical shells. The work is a logical extension of the available perturbation solutions which are of limited use in practical applications. The results generated here are of direct practical use because they cover a wide practical range of the parameters involved. The analysis has also served to establish the range of validity of the perturbation solutions. Charts are presented from which stress concentration factors and stress intensity factors can be directly read.

The differential equation approach does not seem to have been used earlier in the analysis of crack problems in shells. The paper thus provides an interesting alternative to the existing methods particularly when more complicated problems involving, for instance, elasto–plastic analysis are to be solved. Of particular interest should be the "hybrid" technique developed in this paper for satisfying the boundary conditions in a crack problem. The method combines the effectiveness of one type of expansion in satisfying the boundary conditions on the singular components of stresses with that of another in satisfying the overall boundary conditions.

REFERENCES

1. E. M. Mansfield, Neutral holes in plane sheet: Reinforced holes which are elastically equivalent to the uncut sheet, *A.R.C. Tech. Report, R & M*, No. 2815 (1955).
2. F. Erdogan, J. J. Kibler and R. Roberts, Fatigue and fracture on thin-walled tubes containing cracks, *Proc. 1st Int. Conf. on Pressure Vessel Technology*, Delft, The Netherlands, (1969).
3. W. M. Catanach and F. Erdogan, Fatigue crack propogation in cylindrical shells, *Proc. 2nd Int. Conf. on Fracture*, p. 765. Chapman and Hall (1969).
4. A. I. Lurie, Concentration of stresses in the vicinity of an aperture in the surface of a circular cylinder, *Prikladnaya Mathematika i Mekhanika* **10**, 397 (1946), (in Russian).
5. I. A. Shevliakov and F. S. Zigel, The torsion of an empty cylinder with a hole in its side surface, *Dopovidi Ann. U.S.S.R.* **1**, 41–44 (1954).
6. D. Withum, The cylindrical shell with a circular hole under torsion, *Ingr.—Arch.* **26**, 435–446 (1958).

7. J. G. Lekkerkerker, Stress concentration around circular holes in cylindrical shells, *Proc. 11th Int. Cong. of Applied Mechanics*. Springer, Berlin (1964).
8. A. C. Eringen, A. K. Naghdi and C. C. Thiel, State of stress in a circular cylindrical shell with a circular hole, *Welding Research Council Bulletin*, No. 102 (January 1965).
9. P. Van Dyke, Stresses about a circular hole in a cylindrical shell, *AIAA Journal* **3(9)**, 1733–1742 (1965).
10. P. Van Dyke, Stresses in a cylindical shell with a rigid inclusion, *AIAA Journal* **5 (1)**, 125–137 (1965).
11. K. P. Rao, Reinforced holes in shells, Doctoral thesis, Imperial College, London (1969).
12. R. Venkitapathy, Die kreiszylinderschale mit elliptischem Ausschnitt, Dissertation, Technische Hochschule, Hannover, Germany (Nov. 26, 1963).
13. G. N. Savin and A. N. Guz, On the state of stress near curvilinear holes in shells, *NASA Technical Translation, NASA TTF*-423 (May 1966).
14. M. V. V. Murthy, Stresses around an elliptic hole in a cylindrical shell, *J. Appl. Mech.* **36**, 39–46 (March 1969).
15. M. V. V. Murthy and M. N. Bapu Rao, Stresses in a cylindrical shell weakened by an elliptic hole with major axis perpendicular to shell axis, *J. Appl. Mech.* **37**, 539–541 (June 1970).
16. E. S. Folias, A circumferential crack in a pressurized cylindrical shell, *Int. J. Fracture Mech.* **3**, 1–12 (March 1967).
17. M. N. Bapu Rao, and M. V. V. Murthy, On the stresses in the vicinity of an elliptic hole in a cylindrical shell under torsional loading, *Nuclear Engng. and Design* **17**, 309–321 (1971).
18. S. I. Chou, Stress state around a circular cylindrical shell with an elliptic hole under torsion, *J. Appl. Mech.* 534–536 (June 1971).
19. M. N. Bapu Rao and T. Ariman, On the stresses around an elliptic hole in a cylindrical shell, *Acta Mechanica*, **12 (1, 2)**, 1–20 (1971).
20. M. N. Bapu Rao, T. Ariman and L. H. N. Lee, Cylindrical shells subject to uniform bending moment around an elliptic hole, *Int. J. Solids Struct.* **8**, 945–959 (1972).
21. M. V. V. Murthy, K. P. Rao and A. K. Rao, Stresses around an axial crack in a pressurized cylindrical shell, *Int. J. Fracture Mech.* **8(3)**, 287–297 (Sept. 1972).
22. E. S. Folias, An axial crack in a pressurized cylindrical shell, *Int. J. Fracture Mech.* **1**, 104–113 (1965).
23. L. G. Copley and J. L. Sanders, Jr., A longitudinal crack in a cylindrical shell under internal pressure, *Int. J. Fracture Mech.* **5**, 117–131 (1969).
24. M. E. Duncan and J. L. Sanders, Jr., The effect of a circumferential stiffener on the stress in a pressurized cylindrical shell with a longitudinal crack, *Int. J. Fracture Mech.* **5**, 133–155 (1969).
25. F. Erdogan and M. Ratwani, Fatigue and fracture of cylindrical shells containing a circumferential crack, *Int. J. Fracture Mech.* **6(4)**, 379–392 (Dec. 1970).
26. Ole Tingleff, Stress concentration in a cylindrical shell with an elliptical cutout, *AIAA Journal* **9(11)**, 2289–2291 (1971).
27. L. H. Donnel, *NACA Report* No. 479, Washington, D.C. (1933).
28. N. W. McLachlan, *Theory and application of Mathieu Functions*. Oxford University Press (1951).
29. H. P. Mulholland and S. Goldstein, Characteristic numbers of Mathieu's equation with imaginary parameter, *Phil. Mag.* **8**, 834–840, (1929).
30. C. J. Bouwkamp, A note on Mathieu functions, *Kon. Nederl. Akad. Wetensch. Proc.* **51**, 891–893 (1948).
31. M. Abramowitz and I. A. Stegun, *Handbook of Mathematical Functions*, p. 361. Dover Publications, New York, (1965).
32. M. L. Williams, On the stress distribution at the base of a stationary crack, *J. Appl. Mech.* **24**, 109–114 (March 1957).
33. M. L. Williams, The bending stress distribution at the base of a stationary crack, *J. Appl. Mech.* **28**, 78–82 (1961).
34. J. K. Knowles and N. M. Wang, On the bending of an elastic plate containing a crack, *J. Maths. Phys.* **39**, 223–236 (1960).
35. F. A. Leckie, D. J. Payne and R. K. Penny, Elliptical discontinuities in spherical shells, *J. Strain Analysis* **2 (1)**, 34–42 (1967).
36. D. S. Houghton, Stress concentration around cutouts in a cylinder, *J. Royal Aeronautical Soc.* 201–204 (1961).
37. H. Md. Hasseem, A. Subramanian, M. V. V. Murthy and B. Basava Raju, Photoelastic investigations on cutouts in cylindrical and conical shells, *Technical Memorandum*, National Aeronautical Laboratory (to be published).
38. F. Erdogan and M. Ratwani, Fracture of cylindrical and spherical shells containing a crack, *Nuclear Engng. and Design* **20**, 265–286 (1972).
39. G. R. Irwin, Linear fracture mechanics, fracture transition and fracture control, *J. Engng. Fracture Mech.* **1**, 241 (1968).
40. D. S. Dugdale, Yielding of steel sheets containing slits, *J. Mech. Phys. Solids*, **8**, 100 (1960).

41. G. I. Barenblatt, Mathematical theory of equilibrium cracks in brittle fracture, *Adv. Appl. Mech.* **7**, 55 (1962).
42. F. Erdogan and M. Ratwani, Plasticity and the crack opening displacement in shells, *Int. J. Fracture Mech.* **8**, 413–426 (1972).
43. R. B. Anderson and T. L. Sullivan, Fracture Mechanics of through-cracked cylindrical pressure vessels, *NASA TN* D-3252 (1966).
44. A. A. Wells, The status of COD in Fracture Mechanics, *Proc. 3rd Canadian Conf. Appl. Mech.* (1971).
45. A. A. Wells, Crack opening displacement from elastic–plastic analyses of externally notched tension bars, *J. Engng Fracture Mech.* **1**, 399 (1969).
46. F. Erdogan and R. Roberts, A comparative study of crack propogation in plates under extension and bending, *Proc. 1st Int. Conf. on Fracture*, Sendai, Japan **1**, 341 (1965).